



Formation and properties of two-phase bulk metallic glasses by spark plasma sintering

Guoqiang Xie^{a,*}, D.V. Louzguine-Luzgin^b, Akihisa Inoue^{a,b}

^a Institute for Materials Research, Tohoku University, 2-1-1 Katahira, Aoba-ku, Sendai 980-8577, Japan

^b WPI Advanced Institute for Materials Research, Tohoku University, Sendai 980-8577, Japan

ARTICLE INFO

Article history:

Received 11 July 2010

Accepted 5 October 2010

Available online 14 October 2010

Keywords:

Metallic glasses

Spark plasma sintering

Powder metallurgy

Two-phase glassy composites

Microstructure

ABSTRACT

Using a mixture of the gas-atomized $\text{Ni}_{52.5}\text{Nb}_{10}\text{Zr}_{15}\text{Ti}_{15}\text{Pt}_{7.5}$ and $\text{Fe}_{73}\text{Si}_{7}\text{B}_{17}\text{Nb}_3$ glassy alloy powders, we produced the two-phase bulk metallic glass (BMG) with high strength and good soft magnetic properties as well as satisfying large-size requirements by the spark plasma sintering (SPS) process. Two kinds of glassy particulates were homogeneously dispersed each other. With an increase in sintering temperature, density of the produced samples increased, and densified samples were obtained by the SPS process at above 773 K. Good bonding state among the Ni- and Fe-based glassy particulates was achieved.

© 2010 Elsevier B.V. All rights reserved.

1. Introduction

Two-phase metallic glasses (including phase separating metallic glasses) have attracted increasing attention since phase separation might produce metallic glasses with new properties. Recently, such two-phase metallic glasses were successfully produced for different alloy systems by rapid quenching from the alloy melt [1–10]. The requirements for the formation of a two-phase metallic glass alloy are on one hand a high glass-forming ability, on the other hand a strong de-mixing tendency of some components, which is in contradiction with the high glass-forming ability [11]. It is well known that the BMGs are commonly produced by a copper mould casting method so far, and a rather high cooling rate is required during casting to suppress the formation of the more thermodynamically stable crystalline phases. Especially Ni-based glassy alloys [12,13] having high strength of about 2.5–3 GPa exhibit significant size limitations (many of them have a critical diameter below 3 mm, except for Ni–Pd–P alloys). Sample size and shape are seriously limited, thereby limiting the range of their applications.

In order to overcome the disadvantage, the BMGs produced by powder metallurgy process using glassy alloy powders should be a good alternative. Spark plasma sintering (SPS) process, as a novel technique developed for rapid sintering of metals, ceramics and composite materials, has a great potential for sintering amorphous materials [14–16]. The SPS process is a type of compres-

sion sintering technique which is somewhat similar to hot-pressing (HP), so that the sintered samples with a large-size and complicated shape can be produced [14,15]. Recently, we have produced a Ni-based BMG and its composites with a diameter of 20 mm and nearly 100% relative density by spark plasma sintering of gas-atomized $\text{Ni}_{52.5}\text{Nb}_{10}\text{Zr}_{15}\text{Ti}_{15}\text{Pt}_{7.5}$ glassy alloy powder and its mixtures blended with ceramic or metal powders [17–21]. Using a mixture of two kinds of the gas-atomized metallic glassy alloy powders (Ni-based and Fe-based), we successfully fabricated the two-phase glassy BMG composites with ultra-high strength and large-size by the SPS process. It is known that the Ni- and Fe-based BMGs exhibit high thermal stability, ultra-high strength and good corrosion resistance [22–24]. Furthermore, the Fe-based BMGs exhibit excellent soft magnetic properties [23]. In a recent paper, we have reported the sinterability of the two-phase BMG samples by the SPS process at a sintering temperature of 773 K [25]. In this paper, we will focus on the effects of the sintering temperature on the microstructure and properties of the produced BMG samples.

2. Experimental procedures

The glassy powders of the $\text{Ni}_{52.5}\text{Nb}_{10}\text{Zr}_{15}\text{Ti}_{15}\text{Pt}_{7.5}$ and $\text{Fe}_{73}\text{Si}_{7}\text{B}_{17}\text{Nb}_3$ (compositions are given in nominal at.%) alloys are used in this study. Master ingots of the $\text{Ni}_{52.5}\text{Nb}_{10}\text{Zr}_{15}\text{Ti}_{15}\text{Pt}_{7.5}$ and $\text{Fe}_{73}\text{Si}_{7}\text{B}_{17}\text{Nb}_3$ alloys were prepared by arc melting the mixtures of high purity elements in an argon atmosphere purified using Ti getter. The glassy alloy powders were produced by a high pressure argon gas-atomization process. The details of the processing procedure and characterization of the prepared powders have been given elsewhere [17]. Both of the glassy alloy powders used in this study were below 63 μm in size. The morphology of the powders is shown in Fig. 1. The glassy structure behavior of the gas-atomized powders obtained was

* Corresponding author. Tel.: +81 22 215 2492; fax: +81 22 215 2381.
E-mail address: xieq@imr.tohoku.ac.jp (G. Xie).

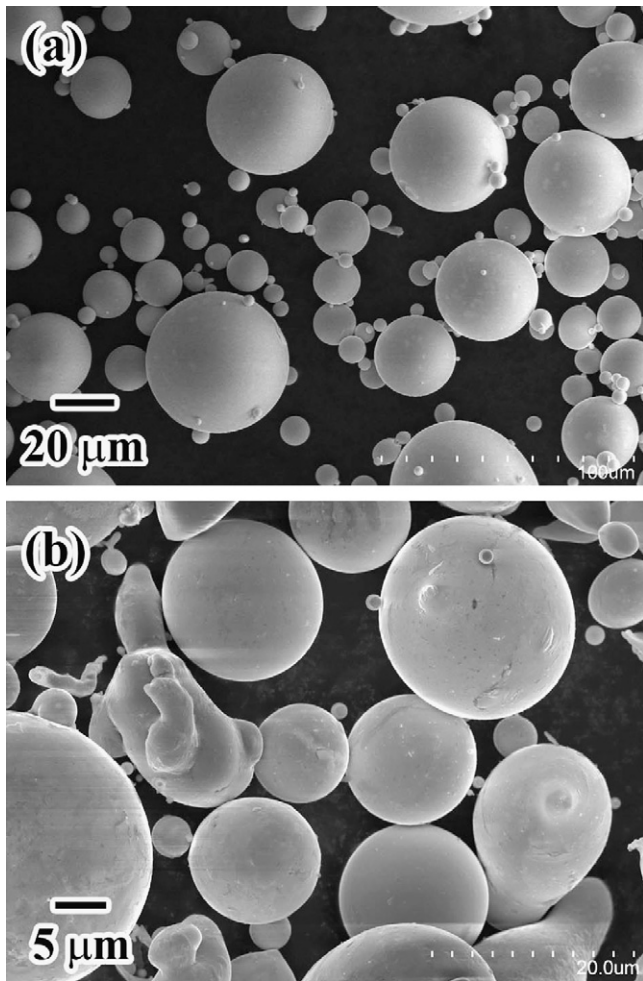


Fig. 1. SEM micrographs of starting powders: (a) the gas-atomized $\text{Ni}_{52.5}\text{Nb}_{10}\text{Zr}_{15}\text{Ti}_{15}\text{Pt}_{7.5}$ alloy powder, (b) the gas-atomized $\text{Fe}_{73}\text{Si}_7\text{B}_{17}\text{Nb}_3$ alloy powder.

demonstrated by X-ray diffractometry (XRD) and differential scanning calorimetry (DSC). Then the two glassy alloy powders having a designated volume ratio (1:1 in this paper) were uniformly blended. The mixed powders were pre-compacted, and then sintered in a vacuum using a SPS apparatus (Model SPS-3.20MK-IV) with

Table 1

Density (ρ) and relative density (ρ/ρ_0) of the two-phase BMG samples sintered by the SPS process at various sintering temperatures.

Sintering temperature (K)	ρ (g/cm^3)	ρ/ρ_0 (%)
748	7.542 ± 0.160	94.19
773	7.918 ± 0.058	98.89
798	8.006 ± 0.002	99.98
	0.011	

a loading pressure of 600 MPa and holding time of 10 min. The details of heating method, temperature measurement and control, as well as loading pressure control in the SPS process have been described in a previous paper [26]. The obtained samples had a cylindrical shape with a diameter of 20 mm and a height of about 5 mm.

The density of the obtained samples was determined by the Archimedeian method using tetrabromoethane. Mechanical properties under uniaxial compression were measured using a conventional mechanical testing machine (Shimadzu, Autograph AG-X) at a constant crosshead speed which corresponds to the initial strain rate of $5 \times 10^{-4} \text{ s}^{-1}$. The samples with a rectangular shape of 2.5 mm in length, 2.5 mm in width and 5.0 mm in height were used. Magnetic properties including saturation magnetization and coercive force were measured with a vibrating sample magnetometer (VSM) and a B-H loop tracer.

The structures of the original powders and the produced samples were examined by XRD in reflection with a monochromatic $\text{Cu K}\alpha$ radiation, while the thermal stability was examined by DSC at a heating rate of 0.67 K s^{-1} . The microstructure was characterized using scanning and transmission electron microscopy (SEM and TEM).

3. Results and discussion

The density of the sintered samples was determined by the Archimedeian method. Table 1 gives the measured density of the samples sintered by the SPS process at various sintering temperatures with a loading pressure of 600 MPa and a holding time of 10 min. The reported density results are from an average value of at least three sintered samples at each sintering temperature. The relative density increases with an increase in sintering temperature and reaches 98.89% at a sintering temperature of 773 K.

Fig. 2(a) shows the XRD patterns obtained from the samples sintered by the SPS process at various sintering temperatures, as well as those of the original Ni- and Fe-based alloy powders. Both original powders exhibit the typical glassy features. No diffraction peaks corresponding to crystalline phases are observed. The XRD intensity profile of the samples sintered by the SPS process at below 773 K shows a superposition of the broad maxima from two glassy phases, as shown in (C) and (D) in Fig. 2(a). The position and

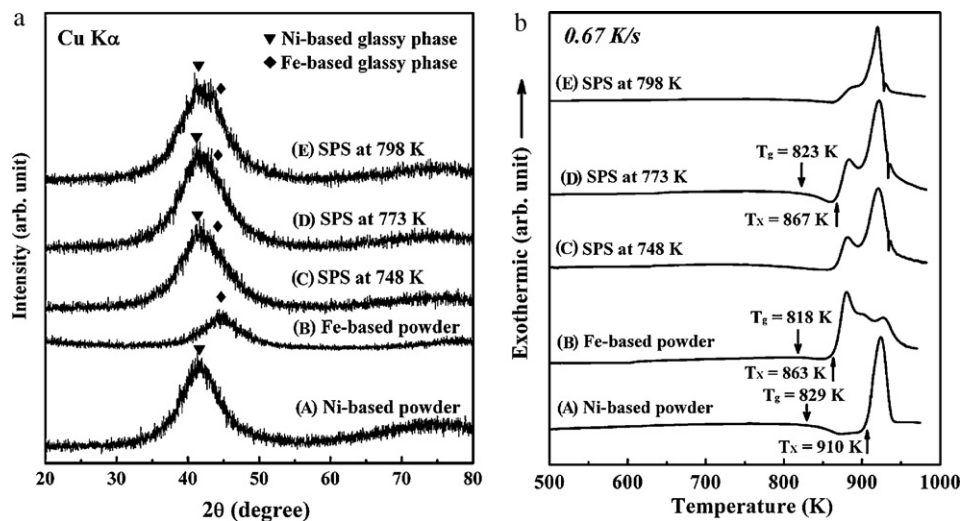


Fig. 2. XRD patterns (a) and DSC curves (b) of the samples sintered by the SPS process at various sintering temperatures. The XRD patterns and DSC curves of the original gas-atomized $\text{Ni}_{52.5}\text{Nb}_{10}\text{Zr}_{15}\text{Ti}_{15}\text{Pt}_{7.5}$ and $\text{Fe}_{73}\text{Si}_7\text{B}_{17}\text{Nb}_3$ alloy powders are also shown for comparison.

the intensity match with those of Ni- and Fe-based glassy phases shown in (A) and (B) in Fig. 2(a), respectively. No other phases are detected within the sensitivity limit of XRD. This indicates that the samples sintered by the SPS process at below 773 K have a two-phase glassy structure of the Ni- and Fe-based glassy phases. On the other hand, the increase in the sintering temperature to over 798 K results in additional appearance of the crystalline peaks, as shown in (E) in Fig. 2(a). This is also confirmed by the DSC measurement. Fig. 2(b) shows the DSC curves obtained from the samples sintered by the SPS process at various sintering temperatures, as well as those of the original Ni- and Fe-based alloy powders. The crystallization behavior of the sintered samples is different from those of the powders. The crystallization of the samples sintered by the SPS process at below 773 K exhibits the combined behavior of both glassy phases. The Fe-based glassy phase starts to crystallize at 867 K, and then is followed by the crystallization of the Ni-based glassy phase, as shown in (C) and (D) in Fig. 2(b). It indicates that no crystallization occurs during the SPS process for the sintering at below 773 K. However, the crystallization enthalpy for the sample sintered at 798 K is smaller than that at below 773 K, as shown in (E) in Fig. 2(b). It should originate from partial crystallization of the sintered sample during the SPS process.

The microstructure of the produced samples was characterized by SEM and TEM. Fig. 3 shows SEM micrographs of the cross section of the samples sintered by the SPS process at various sintering temperatures. A number of pores are observed in the samples sintered at temperatures below 748 K, as shown in Fig. 3(a). The neck formation between powder particles can be seen. The original morphology of the powder particles is maintained, though certain deformation of the powder particles can be observed. Increasing sintering temperature to over 773 K, the sintered sample with a relative density above 98.89% exhibits only a few pores in the SEM image, as shown in Fig. 3(b) and (c). Based on the X-ray energy dispersive spectrometry (EDS) analyses, the light areas belong to the $\text{Ni}_{52.5}\text{Nb}_{10}\text{Zr}_{15}\text{Ti}_{15}\text{Pt}_{7.5}$ glassy phase, while the dark areas represent the $\text{Fe}_{73}\text{Si}_7\text{B}_{17}\text{Nb}_3$ glassy phase in Fig. 3. It is seen that two kinds of glassy particulates are homogeneously dispersed in the sample. The interface among the glassy phases is continuous. Good bonding among the Ni- and Fe-based glassy particulates is presented. The good bonding state between the glassy particulates was also confirmed by the high-resolution TEM observation [25].

Based on the results in Figs. 1 and 3, one can note when the sintering temperature is higher than 773 K, the deformation of the Fe-based alloy particles have been caused, while the Ni-based particles are not deformed. It indicates that the temperature at the contact interfaces between powder particles has reached the super-cooled liquid region temperature of the $\text{Fe}_{73}\text{Si}_7\text{B}_{17}\text{Nb}_3$ glassy alloy. It is known that the SPS process is an electrical sintering technique which applies an ON-OFF DC pulse voltage. The pulse electric current directly flows through the sintered powder materials in the SPS process. Thus the temperature at the contact interfaces between powder particles, especially at low relative density, should be higher than the average temperature for the sintered samples due to the focused current and Joule heat at the bonded interface between powder particles [14,15,27–29], which has been demonstrated in our previous investigations of Al–Mg alloy powders sintered by the SPS process [30–32]. This local high temperature can enhance the formation and growth of the neck between powder particles, and obtain the sintered samples with the excellent properties. Moreover, the sintering temperature was controlled by the die temperature in the present study. It has been demonstrated that the die temperature should be lower than that of metal powder temperature in a SPS process [33,34]. The sintering might be carried out in a temperature over the measured sintering temperature in the SPS process. The produced two-phase glassy samples without

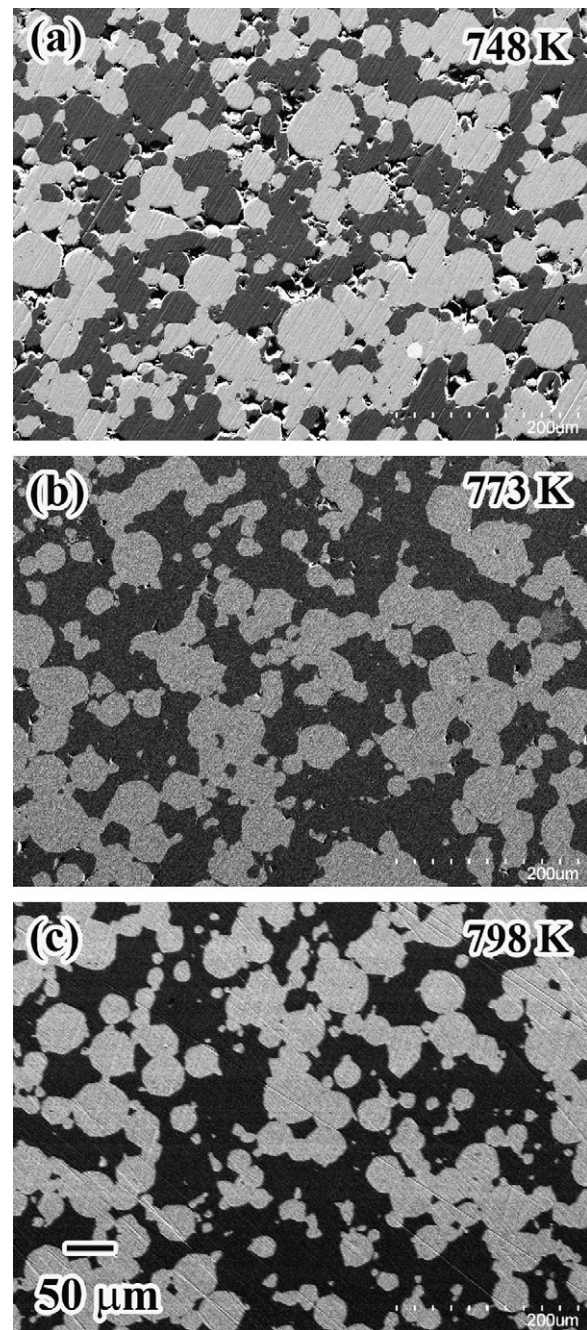


Fig. 3. SEM micrographs of the cross section of the samples sintered by the SPS process at various sintering temperatures: (a) 748 K, (b) 773 K and (c) 798 K.

crystallization and with high strength have been obtained by the SPS process at the sintering temperature of 773 K, which is much lower than the onset temperature of the crystallization (T_x) as well as the glass transition temperature (T_g) of the $\text{Fe}_{73}\text{Si}_7\text{B}_{17}\text{Nb}_3$ and $\text{Ni}_{52.5}\text{Nb}_{10}\text{Zr}_{15}\text{Ti}_{15}\text{Pt}_{7.5}$ glassy alloy powders as shown in Fig. 2(b). We have demonstrated in our previous studies that the crystallization of Zr- and Ni-based BMGs and their composites were avoided upon the SPS process [16–18,35,36]. The significant viscous flow deformation under high pressure at a proper temperature and a certain holding time promotes effective diffusion from one to another glassy phase, and results in continuous connection between the glassy phases (Fig. 3). At the sintering temperature of 798 K which is lower than the T_x as well as T_g of the $\text{Fe}_{73}\text{Si}_7\text{B}_{17}\text{Nb}_3$ glassy powder yet, also lower than those of the $\text{Ni}_{52.5}\text{Nb}_{10}\text{Zr}_{15}\text{Ti}_{15}\text{Pt}_{7.5}$ glassy

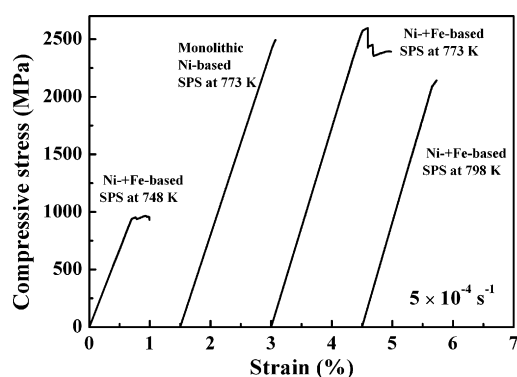


Fig. 4. Compressive stress–strain curves of the samples sintered by the SPS process at various sintering temperatures. The compressive stress–strain curve of the monolithic $\text{Ni}_{52.5}\text{Nb}_{10}\text{Zr}_{15}\text{Ti}_{15}\text{Pt}_{7.5}$ glassy alloy sample sintered by the SPS process at 773 K is also shown for comparison.

Table 2

Some measured mechanical properties of the produced BMG samples sintered by the SPS process at various sintering temperatures.

Sintering temperature, T_s (K)	Ultimate compression stress, σ_{\max} (MPa)	Young's modulus, E (GPa)
748	970	129.0
773	2600	170.4
773 ^a	2490	158.5
798	2140	180.9

^a Monolithic $\text{Ni}_{52.5}\text{Nb}_{10}\text{Zr}_{15}\text{Ti}_{15}\text{Pt}_{7.5}$ compact sintered by SPS process.

powder, the crystallization of the sintered samples took place for the kinetic reasons (Fig. 2(b)).

The compressive properties of the produced samples have been evaluated. Fig. 4 shows nominal compressive stress–strain curves, and Table 2 gives the ultimate compression strength and Young's modulus of the samples sintered by the SPS process at various temperatures, as well as those for the monolithic $\text{Ni}_{52.5}\text{Nb}_{10}\text{Zr}_{15}\text{Ti}_{15}\text{Pt}_{7.5}$ glassy alloy sample sintered by the SPS process at 773 K for comparison. The reported results are an average value of at least three sintered samples at each sintering temperature. The compressive strength for the two-phase BMG sample sintered by the SPS process at a sintering temperature of 773 K is 2600 MPa. It is higher than that of the monolithic $\text{Ni}_{52.5}\text{Nb}_{10}\text{Zr}_{15}\text{Ti}_{15}\text{Pt}_{7.5}$ glassy alloy sample, which is 2490 MPa [17]. However, the strength is not very high for the samples sintered by the SPS process at 748 K and 798 K, this is because the sample sin-

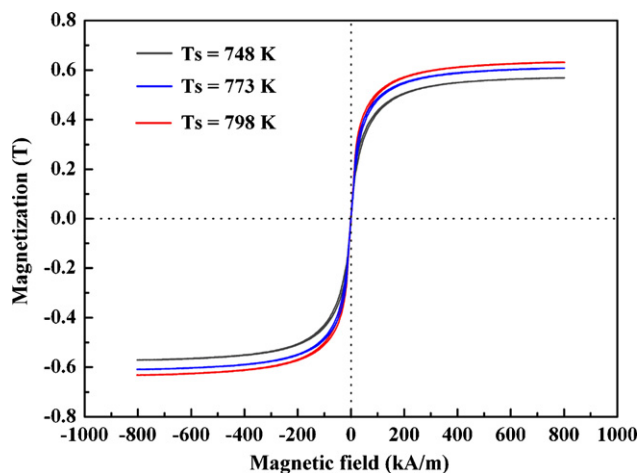


Fig. 5. Hysteresis loop of the samples sintered by the SPS process at various sintering temperatures.

tered at 748 K is not densified (refer to Table 1), and that sintered at 798 K is partially crystallized, as shown in Fig. 2. The good bonding state between the particles and the avoided crystallization of the glassy phases should be responsible for the high strength of the produced two-phase BMG samples, which is mainly originated from the advantage of the SPS process [17].

Fig. 5 shows the magnetic hysteresis loops of the samples sintered by the SPS process at various sintering temperatures. These two-phase BMG samples exhibit excellent soft magnetic properties, which are originating from the randomly dispersed $\text{Fe}_{73}\text{Si}_{7}\text{B}_{17}\text{Nb}_3$ glassy phase. One can note that the saturation magnetization (I_s) of the produced samples increases with an increase in sintering temperature.

4. Conclusions

We have produced the two-phase BMG with high strength and good soft magnetic properties as well as satisfying large-size requirements by the spark plasma sintering of a mixed powder of the gas-atomized $\text{Ni}_{52.5}\text{Nb}_{10}\text{Zr}_{15}\text{Ti}_{15}\text{Pt}_{7.5}$ and $\text{Fe}_{73}\text{Si}_{7}\text{B}_{17}\text{Nb}_3$ glassy alloy powders. Effects of the sintering temperature on the thermal stability, microstructure, mechanical and magnetic properties of the produced two-phase BMGs were investigated. Two kinds of glassy particulates are homogeneously dispersed in each other. The densified samples with a compressive strength of 2600 MPa can be obtained by the SPS process sintered at 773 K. Good bonding state among the Ni- and Fe-based glassy particulates is recognized.

Acknowledgments

The authors sincerely thank Dr. C.T. Chang, Dr. P. Sharma and Professor H. Kimura from Institute for Materials Research of Tohoku University for their helpful support. The work was supported by Grant-In-Aid on "Research and Development Project on Advanced Materials Development and Integration of Novel Structured Metallic and Inorganic Materials" and Grant-In-Aid for Scientific Research (C) (No. 20560639) from the Ministry of Education, Sports, Culture, Science and Technology, Japan.

References

- [1] A. Inoue, S. Chen, T. Masumoto, Mater. Sci. Eng. A 179–180 (1994) 346–350.
- [2] M. Matsuura, M. Sakurai, K. Suzuki, S. Chen, A. Inoue, Physica B 208–209 (1995) 357–359.
- [3] A.A. Kündig, M. Ohnuma, D.H. Ping, T. Ohkuba, K. Hono, Acta Mater. 52 (2004) 2441–2448.
- [4] B.J. Park, H.J. Chang, D.H. Kim, W.T. Kim, Appl. Phys. Lett. 85 (2004) 6353–6355.
- [5] N. Mattern, U. Kühn, A. Gebert, T. Gemming, M. Zinkevich, H. Wendrock, L. Schultz, Scr. Mater. 53 (2005) 271–274.
- [6] J.C. Oh, T. Ohkubo, Y.C. Kim, E. Fleury, K. Hono, Scr. Mater. 53 (2005) 165–169.
- [7] E.S. Park, D.H. Kim, Acta Mater. 54 (2006) 2597–2604.
- [8] T. Wada, D.V. Louzguine-Luzgin, A. Inoue, Scr. Mater. 57 (2007) 901–904.
- [9] E.S. Park, E.Y. Jeong, J.K. Lee, J.C. Bae, A.R. Kwon, A. Gebert, L. Schultz, H.J. Chang, D.H. Kim, Scr. Mater. 56 (2007) 197–200.
- [10] Q.S. Zhang, W. Zhang, G.Q. Xie, A. Inoue, Mater. Sci. Eng. B 148 (2008) 97–100.
- [11] A. Inoue, A. Takeuchi, Mater. Trans. 40 (2002) 1892–1906.
- [12] D.V. Louzguine-Luzgin, T. Shimada, A. Inoue, Intermetallics 13 (2005) 1166–1171.
- [13] D.V. Louzguine-Luzgin, T. Shimada, A. Inoue, Mater. Sci. Eng. A 449–451 (2007) 198–202.
- [14] M. Tokita, Mater. Sci. Forum 308–311 (1999) 83–88.
- [15] V. Mamedov, Powder Metall. 45 (2002) 322–328.
- [16] G.Q. Xie, W. Zhang, D.V. Louzguine-Luzgin, H. Kimura, A. Inoue, Scr. Mater. 55 (2006) 687–690.
- [17] G.Q. Xie, D.V. Louzguine-Luzgin, H. Kimura, A. Inoue, Appl. Phys. Lett. 90 (2007) 241902.
- [18] G.Q. Xie, D.V. Louzguine-Luzgin, H. Kimura, A. Inoue, F. Wakai, Appl. Phys. Lett. 92 (2008) 121907.
- [19] G.Q. Xie, D.V. Louzguine-Luzgin, S. Li, H. Kimura, A. Inoue, Mater. Trans. 50 (2009) 1273–1278.
- [20] G.Q. Xie, D.V. Louzguine-Luzgin, A. Inoue, J. Alloys Compd. 483 (2009) 239–242.

- [21] G.Q. Xie, D.V. Louzguine-Luzgin, H. Kimura, A. Inoue, *Intermetallics* 18 (2010) 851–858.
- [22] A. Inoue, *Acta Mater.* 48 (2000) 279–306.
- [23] A. Inoue, B.L. Shen, *Adv. Mater.* 16 (2004) 2189–2192.
- [24] M. Stoica, K. Hajlaoui, J. Das, J. Eckert, A.R. Yavari, *Rev. Adv. Mater. Sci.* 18 (2008) 23–26.
- [25] G.Q. Xie, D.V. Louzguine-Luzgin, S. Li, H. Kimura, A. Inoue, *Intermetallics* 17 (2009) 512–516.
- [26] G.Q. Xie, O. Ohashi, M. Song, K. Furuya, T. Noda, *Metall. Mater. Trans. A* 34 (2003) 699–703.
- [27] M. Omori, *Mater. Sci. Eng. A* 287 (2000) 183–188.
- [28] Z.A. Munir, U. Anselmi-Tamburini, M. Ohyanagi, *J. Mater. Sci.* 41 (2006) 763–777.
- [29] A. Cincotti, A.M. Locci, R. Orrù, G. Cao, *AIChE J.* 53 (2007) 703–719.
- [30] G.Q. Xie, O. Ohashi, N. Yamaguchi, M. Song, K. Mitsuishi, K. Furuya, T. Noda, *Jpn. J. Appl. Phys.* 42 (2003) 4725–4728.
- [31] G.Q. Xie, O. Ohashi, T. Sato, N. Yamaguchi, M. Song, K. Mitsuishi, K. Furuya, *Mater. Trans.* 45 (2004) 904–909.
- [32] G.Q. Xie, O. Ohashi, N. Yamaguchi, M. Song, K. Mitsuishi, K. Furuya, T. Noda, *J. Mater. Res.* 19 (2004) 815–819.
- [33] U. Anselmi-Tamburini, S. Gennari, J.E. Garay, Z.A. Munir, *Mater. Sci. Eng. A* 394 (2005) 139–148.
- [34] X. Wang, S.R. Casolco, G. Xu, J.E. Garay, *Acta Mater.* 55 (2007) 3611–3622.
- [35] G.Q. Xie, D.V. Louzguine-Luzgin, H. Kimura, A. Inoue, *Mater. Trans.* 48 (2007) 158–162.
- [36] G.Q. Xie, D.V. Louzguine-Luzgin, F. Wakai, H. Kimura, A. Inoue, *Mater. Sci. Eng. B* 148 (2008) 77–81.